

LITHIUM-6-BASED PASSIVE REACTIVITY CONTROL DEVICES FOR A GAS-COOLED FAST REACTOR

FISSION REACTORS

KEYWORDS: *gas-cooled fast reactor, passive reactivity control, lithium injection module*

W. F. G. VAN ROOIJEN,* J. L. KLOOSTERMAN,
T. H. J. J. VAN DER HAGEN, and H. VAN DAM *Delft University of Technology*
Department R3, Physics of Nuclear Reactors, Mekelweg 15, 2629 JB Delft
The Netherlands

Received September 29, 2006
Accepted for Publication December 4, 2006

In this paper passive reactivity control devices for a Generation IV gas-cooled fast reactor (GCFR) are discussed. The proposed devices use liquid ${}^6\text{Li}$ as absorber. The device is triggered by a freeze seal, and upon activation the ${}^6\text{Li}$ is irreversibly introduced into the core region by pressure differences. The device is dubbed the lithium injection module (LIM). Transient thermohydraulic calculations were done using the CATHARE2 code on a simplified thermohydraulic model of GFR600, a 600-MW(thermal) GCFR investigated in the scope of the European GCFR-STREP. The thermohydraulic model uses an accurate model of the ceramic fuel plates and includes natural convection decay heat removal circuits. To properly account for power production during the transient, a synthetic decay power curve was made based

on the ANSI/ANS-5.1-1994 law. Loss-of-flow and control rod withdrawal/ejection transients are presented. Neutronic calculations show that the LIMs have a low reactivity worth between -2.1 and -1.5 $\$$. In spite of their low worth, the LIMs are capable of keeping the reactor power bounded during all calculated transients. Shutdown is not always achieved, depending on the kind of transient under consideration. For pressurized loss of flow, recriticality due to Doppler feedback may become problematic in the natural-circulation phase. For rapid control rod ejections, the resulting very fast power transients cause concern for material degradation. One LIM would be enough to control reactor power, but redundancy may call for more than one LIM in the core.

I. INTRODUCTION

In this paper, options for passive reactivity control of a Generation IV gas-cooled fast reactor (GCFR) are discussed. The GCFR is one of the six reactor concepts selected by the Generation IV International Forum, envisaged to enter service halfway into the 21st century.¹ The reference Generation IV GCFR is a helium-cooled reactor, with high outlet temperature (850°C) and electricity production in a direct Brayton cycle. The target power density in the core is ~ 100 MW/m³, with a large fraction of coolant (55%) in the core to decrease coolant friction. The high power density (for a gas-cooled system), in combination with a low thermal inertia in the core [no large graphite volume in the core like in high-temperature reactors (HTRs)], and low effective delayed

neutron fraction (uranium-plutonium fuel) open the potential for rapid, high-temperature transients. Within the current European FP6 GCFR-STREP,^a our task is to evaluate the impact of adding extra minor actinides (MAs) to the reference fuel for transmutation purposes. Adding extra MAs decreases the effective delayed neutron fraction and the magnitude of the Doppler coefficient. To counteract these effects a passive reactivity control device has been designed to limit power production of the reactor under transient situations.

The proposed device, the lithium injection module (LIM) uses liquid ${}^6\text{Li}$ as a working fluid. It is shown in Sec. III.A that the device can be made small enough to be integrated into the regular control assemblies. In Secs. IV and V, the thermohydraulic model of the reactor and the

*E-mail: w.f.g.vanrooijen@tudelft.nl

^aEuropean Commission/EURATOM Sixth Framework Programme GCFR Specific Targeted Research Programme.

decay heat model are described. Transient calculations presented in Sec. VI on an unprotected loss-of-flow accident (LOFA) and control rod withdrawal (CRW) show that the LIM can limit the power output of the reactor, although shutdown is not always achieved. The LIMs can decrease the risk of unprotected transients and thereby increase the safety level of the GCFR.

II. PASSIVE REACTIVITY CONTROL: OPTIONS AND CONSTRAINTS

To shut down a nuclear reactor, three options are generally available:

1. Introduce a parasitic absorber.
2. Increase leakage from the reactor.
3. Remove the fuel, or reshape the fuel into a less reactive configuration (possible in mobile fuel reactors, e.g., molten salt reactor, pebble bed reactor).

Option 1, the introduction of an absorber, is commonly used to control nuclear reactors. The device under investigation is intended to operate in the early phases of an unprotected transient because as will be shown later, the Doppler effect is usually not very strong in a GCFR, resulting in high fuel temperatures and possibly damage. The first decision to be made for passive devices is which parameter should provide the activation signal. In a first design step, it was decided to use the reactor pressure as the governing parameter. This was motivated by the fact that a loss-of-coolant accident (LOCA) in a high-power core would have severe effects: Temperatures in the core will increase due to a lack of cooling, and the void coefficient may be positive for a GCFR. Pressure-operated passive reactivity devices for gas-cooled reactors were investigated earlier, e.g., see Refs. 2 and 3. However, pressure-operated devices are not practical for several reasons:

1. There will be a pressure holding system on the primary circuit, which will keep pressure more or less constant, also during the beginning of a transient.
2. A change of the reactor power level may introduce pressure variations in the primary circuit. Depending on the power conversion system (PCS), power output may be controlled by adjusting the flow (direct cycle system) or inventory (indirect cycle system, considered as a backup option), leading to pressure fluctuations. If the reactor is intended for load-following, the design pressure in the primary system may have a large range.
3. Pressure-operated devices using the absolute system pressure need to be disarmed in case of an intended depressurization. These intended depressurizations might occur during maintenance and refueling for instance, when

it is advantageous to use a lower than nominal operation pressure in the primary system.

The passive device presented in Ref. 2 uses the steady-state pressure difference between the inlet and the outlet plenum to lift a control rod above the core, which then drops in case of loss of flow and/or coolant. However, this device is intended to keep the reactor subcritical long after the onset of the transient, relying on Doppler feedback only during the initial phase of the transient. It will be shown that for the GCFR, Doppler feedback only results in unacceptable fuel temperatures.

The risk of a depressurization is quite small, and at the same time there are other events that may lead to reactor damage. Therefore, it was decided to design passive devices using the core outlet temperature as the governing parameter. The rationale for this choice is the following: An accident is basically an unintended mismatch between power production and power removal from the core, and any accident will thus manifest itself as a change of outlet temperature, assuming that the inlet conditions are not directly affected by the accident. The activation temperature of the device can be tuned by using a material with the required melting point, which should have some margin over the maximum design temperature during normal operation and intended transients. A temperature-controlled device can be designed to not require disarming for refueling, etc. For the proposed passive shutdown devices to be successfully integrated into the design of the nuclear reactor, the following demands and constraints are taken into account:

1. The passive device is intended to limit the reactor power under accidental conditions when all other active control systems have failed.
2. The device should be small enough to not interfere with other control systems in the reactor and should preferably be integrated into the regular control assemblies. The assemblies housing passive devices should not be higher than regular assemblies. The background for this is the following: Refueling of a GCFR will be done under (partial) pressurization; hence, all openings through the reactor pressure vessel (RPV) are kept as small as possible. All fuel assemblies are removed vertically through a central hole in the top of the RPV. Thus, to be able to replace each assembly, the assemblies are lifted from their diagrid positions, then moved horizontally to the center of the reactor, and unloaded. Thus, the height above the core should be at least as high as the tallest subassembly.
3. The GCFR under investigation in our cooperation has upward flow through the core. For that reason, suspending a control rod with a Curie-point magnet or similar device would mean that the rod is subject to very hot helium for a long time, which could degrade the reliability of the SCRAM system (self-welding can

be a problem). Also, the GCFR with its high power density (20 times higher than the HTR) has a high helium flow velocity, meaning that the rod suspension mechanism needs to be structurally strong, complicating fuel handling. All upward-flow GCFR designs have control rod insertion from the bottom of the core.

4. Other options to suspend an absorber above the core have been studied, e.g., a fluidized bed of B_4C particles. During steady state, the particles are blown into a knockout vessel above the core region, and if a loss of flow and/or coolant occurs, the particles drop into the core by gravity. This solution was dismissed because of the required volume of the knockout vessel above the core. Another problem is that a reactivity-initiated transient is hard to detect with this system and it would be difficult to avoid depletion of the B_4C particles during normal operation.

5. Even though the passive device is to be integrated into a control assembly, the temperature-sensitive element should be in the outlet gas stream of a fuel assembly to adequately detect the hot gas outlet temperature.

6. The reactivity effect of the passive devices should be so large that activation of only one device will introduce a sufficient amount of negative reactivity.

The last item follows from the behavior of the well-known point kinetics equations for the time-dependent neutron flux (or power) in a nuclear reactor.⁴ Consider the constant decay source approximation of the point kinetics equations in an initially critical reactor:

$$P_n(t) = P_n(0) \exp\left(\frac{\rho - \beta}{\Lambda} t\right) + P_n(0) \frac{\beta}{\beta - \rho} \left\{ 1 - \exp\left(\frac{\rho - \beta}{\Lambda} t\right) \right\}, \quad (1)$$

where

$P_n(t)$ = time-dependent neutronic power

ρ = externally introduced reactivity

β = effective delayed neutron fraction

Λ = neutron generation time.

For $\rho < \beta$, the exponentials on the right side decay quickly, and the power immediately after the reactivity insertion is approximately given by the prompt jump approximation (prompt drop if negative reactivity introduced):

$$P_n(0^+) = \frac{\beta}{\beta - \rho} P_n(0^-), \quad (2)$$

where $P_n(0^-)$ is the steady-state power before the start of the transient and $P_n(0^+)$ is the power immediately after introduction of the reactivity. The amplitude of the prompt jump equals

$$P_n(0^+) - P_n(0^-) = \frac{\rho}{\beta - \rho} P_n(0^-). \quad (3)$$

If the reactivity ρ introduced by the LIM is large, negative, and introduced in a stepwise manner, the power level of the reactor decreases immediately. The magnitude of the prompt jump increases with the magnitude of the LIM reactivity. Once the prompt jump has occurred, the outlet temperature of the coolant will decrease rapidly. If several identical temperature-controlled passive devices are present, their activation is a stochastic process due to fabrication tolerances, etc. One LIM will be the first to respond to the transient, and the resulting prompt jump causes a rapid decrease of reactor power. Thus, the other LIMs may not be activated.

III. INTRODUCTION OF GFR600

All calculations presented in this paper concern GFR600, a 600-MW(thermal) Generation IV GCFR. The main design features are hexagonal fuel assemblies with plate fuel, fully ceramic cladding and structures (SiC), Zr_3Si_2 reflector, a core power density of 103 MW/m^3 , and high-temperature operation between 480 and 850°C. In Table I some key design data are summarized, while Fig. 1 gives an illustration of a GFR600 fuel element. Table II gives the fuel composition of the reference fuel and a fuel with extra MA loading, and Table III finally states the dynamic parameters for the MA fuel.

TABLE I
GFR600 Core Parameters

Power [MW(thermal)]	600
Coolant	He
Power density (MW/m^3)	103
Specific power (W/g HM)	45
$T_{core,in}$ (°C)	480
$T_{core,out}$ (°C)	850
Core H/D (m)	1.95/1.95
Pressure (MPa)	7.0
Fuel type	Plates
Fuel material	UPuC + MA
Structural material	SiC
Reflector material	Zr_3Si_2
Volume percent coolant/structures/fuel	55/10/35

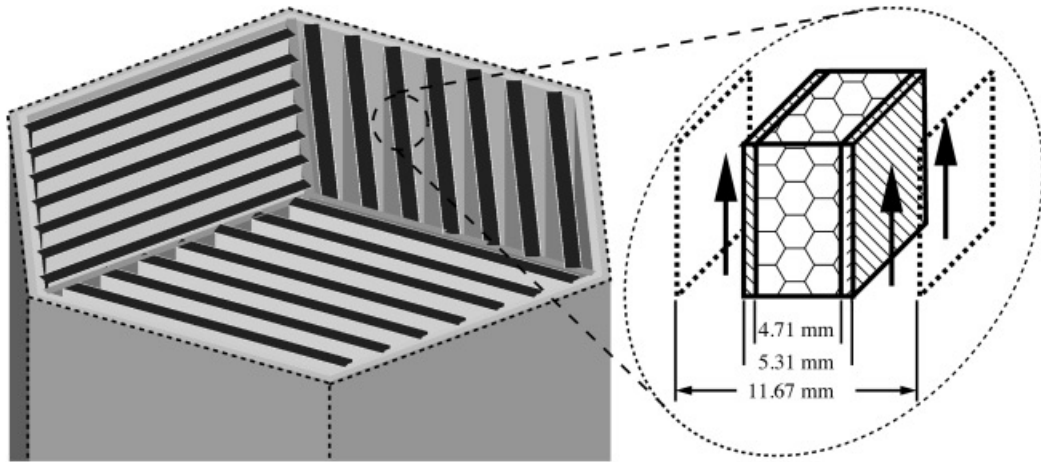


Fig. 1. GFR600 fuel assembly. The light-colored wrapper and central mechanical restraint are made of SiC. The darker fuel slabs contain the fuel mixture clad with SiC. The overall volume fractions are 55 vol% helium, 10 vol% SiC for structures and cladding, and 35 vol% fuel/matrix.

TABLE II
GFR600 Fuel Compositions: Reference Fuel and a Fuel Containing 5% MAs

		Reference Fuel		MA Fuel
Elemental Composition				
U		84%		79%
Pu		16%		16%
MA		—		5%
Isotopic Composition				
	Atomic Density (b·cm) ⁻¹	Atomic Percent	Atomic Density (b·cm) ⁻¹	Atomic Percent
²³⁵ U	1.1631e-4 ^a	0.60	1.0938e-4	0.56
²³⁸ U	1.6291e-2	83.52	1.5320e-2	78.60
²³⁷ Np	—	—	1.6242e-4	0.83
²³⁸ Pu	8.3625e-5	0.43	8.3625e-5	0.43
²³⁹ Pu	1.7395e-3	8.92	1.7395e-3	8.92
²⁴⁰ Pu	8.0163e-4	4.11	8.0163e-4	4.11
²⁴¹ Pu	2.2940e-4	1.18	2.2940e-4	1.18
²⁴² Pu	2.2235e-4	1.14	2.2235e-4	1.14
²⁴¹ Am	2.1687e-5	0.11	6.0680e-4	3.11
^{242m} Am	—	—	2.2072e-6	0.01
²⁴³ Am	—	—	1.5020e-4	0.77
²⁴² Cm	—	—	1.9219e-7	0.001
²⁴³ Cm	—	—	7.0178e-7	0.004
²⁴⁴ Cm	—	—	4.9558e-5	0.254
²⁴⁵ Cm	—	—	1.2086e-5	0.062
²⁴⁶ Cm	—	—	9.4528e-7	0.005

^aRead as 1.1631 × 10⁻⁴.

TABLE III

Dynamic Parameters and Reactivity Coefficients for GFR600, for the Reference Fuel and a Fuel with 5% MAs*

	Reference Fuel (No MAs)	MA Fuel 0% FIMA ^a	MA Fuel 9.3% FIMA
β (pcm)	395.4	373.7	348.2
Λ (s)	$7.5e-7^b$	$7.5e-7$	$7.5e-7$
FTC (pcm/K)	-0.92	-0.56	-0.47
Void coefficient (pcm/69 bars)	+290	+406	+435.6

*See the composition in Table II. FTC expressed as $\Delta\rho/\Delta T$ (pcm/K). Void coefficient is reactivity difference between 70 bars and 1 bar, expressed in pcm per 69 bars.

^aFIMA = fissions per initial metal atom.

^bRead as 7.5×10^{-7} .

III.A. Neutronic Design of Passive Reactivity Control for GFR600

The GFR600 core contains 112 fuel assemblies, 6 control assemblies, and 3 shutdown assemblies and is surrounded by 210 reflector assemblies (Zr_3Si_2 reflector). Neutronic calculations were done using the CSAS26 sequence of SCALE 5 (Ref. 5), which uses a KENO-6 Monte Carlo calculation for criticality. The fuel assemblies are represented by cell-homogenized mixtures (i.e., self-shielding is taken into account). The reflectors are represented as homogeneous mixtures without any lattice effect, and the absorbers are modeled in their actual geometry using a cell calculation to correct the cross sections for effects of absorber self-shielding. For fuel temperature coefficient (FTC) and void calculations, the cell calculations are done separately. Delayed neutron production and decay, and the generation time were calculated using VAREX (Ref. 6) on the unit cell level (one slab of fuel plus coolant).

To make a temperature-controlled passive introduction of reactivity, a device with a freeze seal is chosen. Once the freeze seal melts because of overheating, an absorber is irreversibly released into the core region. The selected absorber is 6Li because it is a strong absorber and liquid at GFR600 operating temperatures. As a liquid, the absorber can be moved easily by pressure differences. The resulting device is similar to the LIM proposed for the RAPID reactor.⁷ A preliminary design was made of an LIM: Seven SiC tubes are filled with 6Li in case of off-nominal conditions. A total of four LIMs are present; their locations will be discussed later. The storage tank containing the 6Li during normal operation is located in the bottom of the assembly. In activated mode, the Li should occupy the fueled length of the core (1.95 m). The inner diameter of the SiC pins is chosen as 22 mm, giving a required volume of 6Li of 5200 cm³ for the seven pins. The size of the storage tank in the bottom of the assembly should allow for the

regular control elements to be operable. The height (axial direction) of the storage tank is chosen as 45 cm, giving a required surface area for the tank of ~ 116 cm². This corresponds to $\sim 50\%$ of the cross flats surface area within the control assembly. It is expected that this leaves enough room for the regular control elements to be operated. Proper shielding of the 6Li is maintained because the height of the shielding in the bottom of the assembly is ~ 120 cm, leaving ~ 75 cm of absorber/reflector above the storage tank. The seven SiC tubes occupy $\sim 13.7\%$ of the volume of the assembly, so enough room is left over for the regular control rods and mechanisms.

The reactivity worth of the LIMs was calculated for several permutations: no LIMs active, one LIM active in the central position of the core, one LIM active in an off-center position, and all four LIMs active. The reactivity worths are given in Table IV.

The LIM is illustrated in Fig. 2. The seven SiC tubes are connected to a plenum at the very top of the assembly. From this plenum, tubelets are protruding sideways into the hot outlet gas stream of the neighboring fuel assemblies. These tubelets contain a small freeze seal of a material with the required melting temperature. Candidate materials for the freeze seals could be silver ($T_m = 962^\circ C$) or gold ($T_m = 1064^\circ C$, maybe adding some alloying element to lower the melting point). The governing parameter to melt the seal is the latent heat of melting. An order of magnitude calculation for a cylindrical freeze seal of 1-cm diameter and 5-mm thickness has shown that the "worst case" time to melt is ~ 10 s, for a temperature difference of 66 K between the helium and freeze seal. The time to melt will be shorter in practice, because the temperature difference will become larger during the transient, and the seal will break before a full melt is achieved. Thus, the seal material should have an adequate melting temperature and low latent heat, and the mass should be minimized. The fabrication of the freeze seal should be as uniform as possible. If one of the freeze

TABLE IV
The Reactivity Effects of the LIMs*

	k_{eff}	ρ	ρ/β	$\Delta\rho/\beta$
Fresh Fuel				
Zero LIMs	1.02432 ± 0.00027	0.0237	6.35	—
One LIM, center	1.01613 ± 0.00023	0.0159	4.25	-2.1
One LIM, off center	1.01848 ± 0.00026	0.0181	4.86	-1.49
Four LIMs	0.99922 ± 0.00023	$-7.8e-4$	-0.21	-6.56
Average Burnup 9.33% FIMA ^a				
Zero LIMs	1.01373 ± 0.00022	0.0135	3.89	—
One LIM, center	1.00587 ± 0.00025	0.0058	1.68	-2.21
One LIM, off center	1.00826 ± 0.00029	0.0082	2.35	-1.54
Four LIMs	0.98868 ± 0.00025	-0.011	-3.29	-7.18

*Each LIM contains seven tubes with ⁶Li, $r_{in} = 1.1$ cm, $r_{out} = 1.2$ cm. The LIM worth increases with burnup, which is mainly contributed to the decrease of β : from 373.7 to 348.2 pcm.

^aFIMA = fissions per initial metal atom.

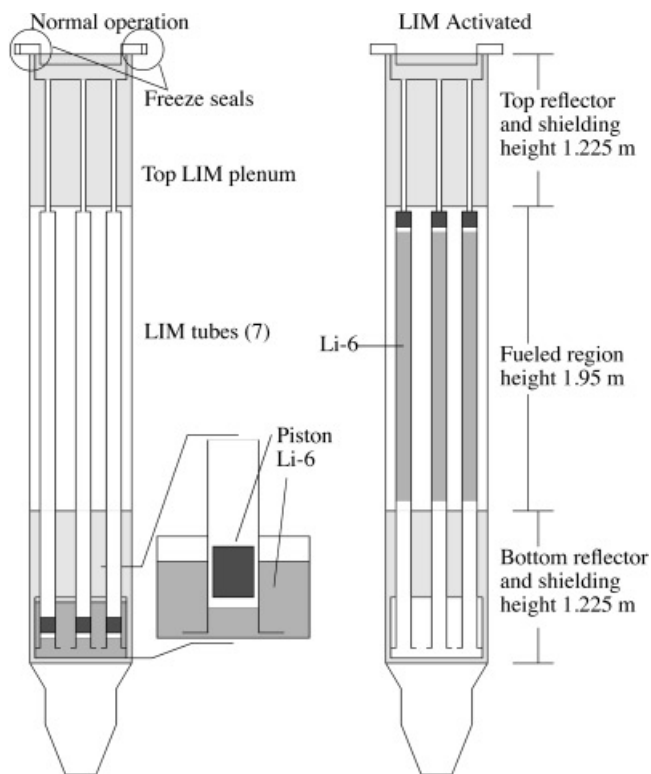


Fig. 2. Rough design of an LIM, activated by a freeze seal (not to scale). The height of the storage tank is ~45 cm. When the LIM is activated, the small SiC pistons seal off the tubes to prevent the ⁶Li from spraying into the reactor.

seals ruptures, the ⁶Li shoots up in the tubes, into the fueled region of the core. The storage tank should be adequately pressurized to move the ⁶Li from the tank into the fueled region of the core [tank pressure at least several bars above the system pressure relieve valve, ~80 bars (8.0 MPa)]. The seven tubes with ⁶Li are equipped with small SiC pistons to seal off the top of the tube in order to prevent the ⁶Li from spraying into the core after activation. These small sealing pistons should have a “one-way” operation: Once they have moved to the top of the assembly, they should stay there rigidly to make sure that the ⁶Li is not pushed back into the storage tank if the reactor pressure increases. A layout of the GFR600 core with the LIM assemblies is shown in Fig. 3. The locations of the LIMs are chosen to obtain the largest number of fuel assemblies connected to an LIM assembly. Each LIM is connected to six neighboring fuel assemblies, with the freeze seal protruding into the hot outlet gas stream of the fuel assemblies. From this configuration some important design issues are identified:

1. If a localized transient occurs, one LIM will be activated, and the power goes down. The other LIMs will not be activated unless the transient inserts more reactivity than the worth of one LIM.

2. LIMs respond to events in only one of the connected fuel elements. If the LIMs are to detect highly localized events like a flow blockage, each fuel assembly should be connected to at least one LIM.

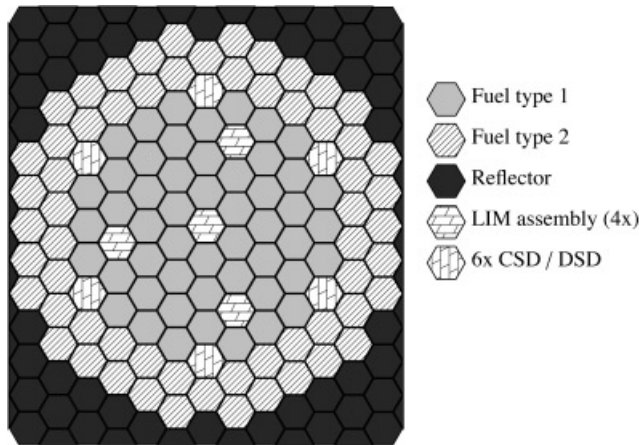


Fig. 3. The layout of the GFR600 core with LIMs. The locations of the LIMs are chosen to obtain the largest number of fuel assemblies connected to an LIM.

3. The freeze seals have to be as uniform as possible in order to activate the largest number of LIMs for a given transient.

III.B. Remarks

In Ref. 8, four categories of passivity (“A” through “D”) are defined for components and systems of a nuclear reactor. The proposed LIM would fall into category “C”: “no signal inputs, no external power source or forces; with moving mechanical part(s) and/or moving working fluid; fluid movement due to thermohydraulic conditions.” From Fig. 2 it is seen that it is advantageous if the column of Li can be pushed up into the fueled region as illustrated in Fig. 2. In this way, the required volume of ${}^6\text{Li}$ is smaller than when the entire length of the tube to the bottom of the storage tank is filled with lithium. A column of a dense fluid can be maintained over a less dense fluid if the diameter of the tube is small enough. The characteristic tube size is given by the limit for the so-called Rayleigh-Taylor instability.⁹ An order of magnitude calculation shows that for the lithium-helium interface, the characteristic size is ~ 50 mm. Since an inner diameter of 22 mm has been chosen, it is concluded that the liquid lithium can be suspended.

The proposed device may be slow to respond to a large-break LOCA (LB-LOCA), as the expanding helium will cool the core, until all coolant is gone and the full void reactivity is inserted. However, as illustrated in Ref. 10, LB-LOCA is always problematic for GCFRs, even if the core is adequately scrammed. Special measures are always necessary to evacuate the decay heat under depressurized conditions. In that sense, LB-LOCA is the Achilles’ heel of the GCFR concept. For reasons discussed later, for the present investigations, LB-LOCA is not considered. The LIM devices could be

made LOCA-sensitive by including a rupture foil next to the freeze seals, to break if the system pressure is too low, and in fact, the freeze seal could probably be engineered to function as rupture disks as well.

The main drawback of the LIMs is that they are specifically one-way systems. After activation, the primary system would have to be inspected for traces of freeze seal material and potentially some ${}^6\text{Li}$. For that reason, the LIMs should be considered as a reactivity control device when all else fails. Because the freeze seals “stick out” into the fuel assemblies, the LIM assemblies have to be removed for refueling. This should not be problematic, as eight other control/shut down assemblies remain.

IV. GFR600 PRIMARY SYSTEM LAYOUT

IV.A. General System Layout

Figure 4 gives an overview of the main design features of the primary system of GFR600. Figure 4 is quite generally applicable for all Generation IV GCFRs, all of which have a similar system layout. Cold helium enters through the annular cross duct and flows down through the downcomer into the lower plenum and into the fuel

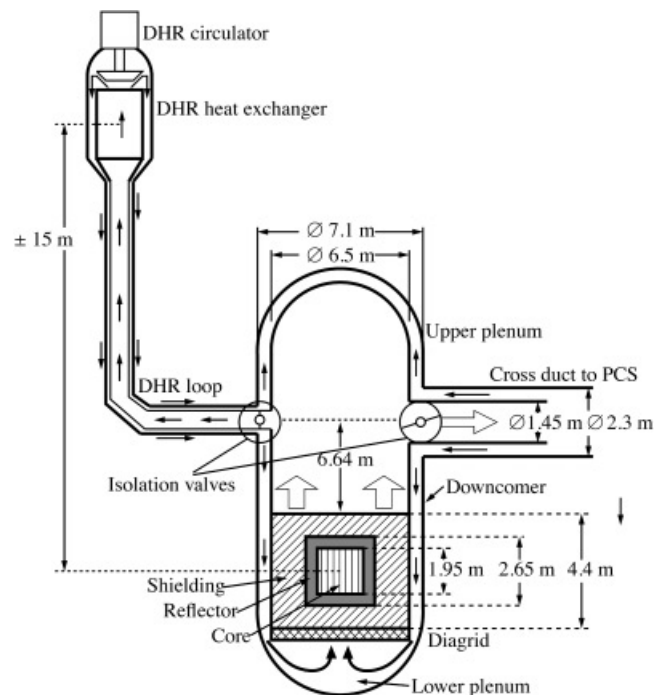


Fig. 4. Layout of the primary circuit of GFR600 (schematic, not to scale). One of the three redundant DHR circuits is shown. To control the flow of coolant, there are valves between the DHR circuits, the main RPV, and the main cross duct.

assemblies. The flow distribution of the coolant over the individual assemblies is done with flow gags on each assembly. The upper plenum is a large volume filled with hot helium, with the hot leg of the cross duct connected to it, as well as three decay heat removal (DHR) loops. To protect the RPV from the hot coolant, the entire primary circuit is laid out as cross ducting, with cold helium flowing between the outer RPV and an inner isolation liner. The RPV thickness is 75 mm, and the vessel material is, depending on the operating temperatures and conditions, 9Cr1Mo steel, or stainless steel.^{11,12}

IV.B. DHR Strategy

The DHR strategy envisaged for GFR600 is similar to other Generation IV GCFR designs. Under pressurized conditions natural circulation of the coolant through the DHR circuits should be sufficient for DHR. To ensure adequate natural circulation, a large elevation between the core midplane and the DHR heat exchanger of ~ 15 m is chosen. Also, the fuel elements are designed to introduce a minimal amount of hydraulic friction. The DHR loops are designed to each extract 3% of the nominal reactor power. During normal operation measures have to be taken to isolate the DHR circuits from the primary coolant flow using valves. Thus, according to Ref. 8, the natural-circulation DHR loops qualify as category “D”: “*Execution of the safety function through passive methods; but using an external signal to initiate the process (opening of valves, etc.)*.” Note that the valves should be “*suitably qualified*,” according to the International Atomic Energy Agency specifications. The DHR isolation valves are located on the cold legs of the DHR circuit.

To obtain an adequate flow through the core and DHR circuits under depressurized conditions, a small DHR circulator is present. The entire primary system is to be surrounded by a “close containment,” which should maintain a backup pressure of ~ 10 to 15 bars under all circumstances. The required pumping power for the DHR circulators will then be so small that they can be driven on battery power for 24 h (according to Ref. 8 such devices are not rated “passive”).

The DHR loops reject heat to a secondary DHR circuit with water as the working fluid. From this loop, heat is transferred to the atmosphere as the final heat sink. The secondary DHR loop relies completely on natural convection. To drive the natural circulation in the secondary DHR loop, the elevation difference between the midplane of the He-H₂O heat exchanger and the heat exchanger to the atmosphere is ~ 5 m.

IV.C. Thermohydraulic Model

The primary circuit of Fig. 4 was modeled using the CATHARE2 code.¹³ This code [CATHARE2 v2.5 mod3.1,

developed by Commissariat à l’Energie Atomique (CEA), Electricité de France, Framatome-ANP, and Institut de Radioprotection et de Sûreté Nucléaire] is a two-phase implicit transient thermal-hydraulics code, able to perform calculations on helium-cooled reactors. Because a detailed description of the PCS does not exist, the inlet and outlet of the reactor are described as boundary conditions. These boundaries are as indicated in Table I, i.e., inlet temperature, 480°C; outlet temperature, 850°C; outlet pressure, 70 bars; helium mass flow, 312 kg/s. The fuel plates are modeled as flat plates in which power is produced. The CATHARE2 model (Fig. 5) has six fuel structures, each representing one ring of fuel assemblies. The axial power profile has a cosine shape with a power peaking of 1.3; radial power peaking is 1.15. The bypass flow between the fuel elements, as well as the flow in the reflector, is currently not modeled. The flow gags on the fuel elements are set up to obtain a uniform outlet temperature of 850°C. Heat exchanges between the vessel and the surrounding environment are not taken into account, because of a lack of detailed design.

The PCS potentially has a large effect on any transient in the GCFR. In Ref. 10 a GCFR with a direct cycle gas turbine is reported. The most important effect of the PCS is that it will keep spinning because of its inertia, improving heat transfer in the primary system. Reference 10 also indicates that in fact premature stopping of the turbocompressor should be avoided and that a typical time for the braking system to completely halt the turbocompressor would be ~ 200 s. If the turbocompressor is allowed to run down by itself, flow will be maintained for a longer period, and the temperatures will change more gradually in the transient. The LIMs would still be activated if the helium temperature reaches an unacceptable level.

V. CALCULATION OF REACTOR POWER DURING A TRANSIENT

The total thermal power of a nuclear reactor is due to power released by fissions (fission power) and partly due to the decay of radioactive fission products (the residual or decay power). The decay power is commonly described as the time-dependent power following one fission in isotope j as

$$f(t) = \sum_{k=1}^K \gamma_{jk} \exp(-\mu_{jk} t) . \quad (4)$$

This formulation assumes that all fission products can be grouped into K groups. Each group has a decay constant μ_{jk} and a contribution γ_{jk} to the total decay power. Decay heat standards based on Eq. (4) include the following standards: ANSI/ANS-5.1-1994 with $j = 4$, $k = 23$ (Ref. 14); DIN 25463-1 with $j = 4$, $k = 24$

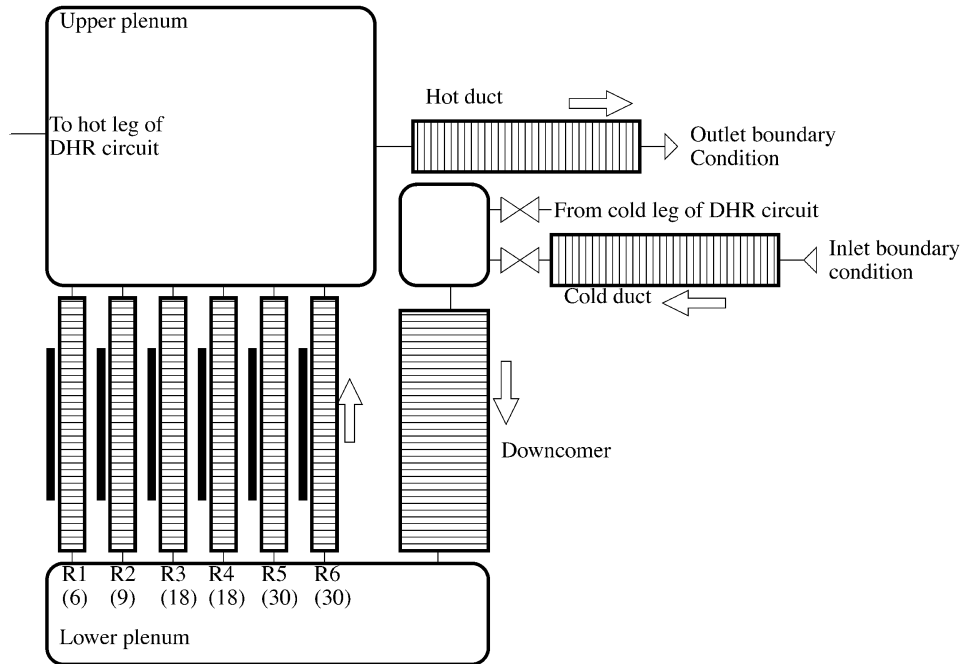


Fig. 5. Illustration of the CATHARE2 model of the GFR600 primary system.

(Ref. 15); or JAERI-1320 with $j = 5, k = 33$ (Ref. 16). The function $f(t)$ is an impulse response and can be extended to an arbitrary fission rate history $\psi(t)$ by convolution to find the decay heat at time t_0 :

$$P_d(t_0) = \int_0^{t_0} \psi(t - \tau) f(\tau) d\tau \quad (5)$$

The convolution Eq. (5) can be rewritten as a differential equation. Doing so, a coupled set of differential equations is found to describe the time-dependent power of a nuclear reactor:

$$\frac{dP_n(t)}{dt} = \frac{\rho(t) - \beta(t)}{\Lambda(t)} P_n(t) + \frac{1}{\Lambda_0} \sum_{i=1}^6 \lambda_i \zeta_i(t) \quad (6)$$

$$\frac{d\zeta_i(t)}{dt} = \frac{F(t)}{F_0} \beta_i(t) P_n(t) - \lambda_i \zeta_i(t) \quad (7)$$

$$\frac{d\epsilon_{jk}(t)}{dt} = C_c f_j \frac{\gamma_{jk}}{\mu_{jk}} \psi(t) - \mu_{jk} \epsilon_{jk}(t) \quad (8)$$

and

$$P_d(t) = \sum_{j=1}^J \sum_{k=1}^K \mu_{jk} \epsilon_{jk}(t) \quad (9)$$

where

$P_n(t)$ = neutronic power (due to fissions)

$\beta_i(t)$ = effective delayed neutron fractions of each delayed neutron precursor group ($\beta(t) = \sum_{i=1}^6 \beta_i(t)$)

$\Lambda_0, \Lambda(t)$ = steady-state and transient neutron generation time

$\zeta_i(t)$ = precursor concentrations for delayed neutrons, with λ_i the corresponding decay constants

$F_0, F(t)$ = steady-state and transient fission rate

$\epsilon_{jk}(t)$ = pseudo decay power

C_c = factor allowing a conservative calculation of the decay heat power if set to >1.0

f_j = fraction of fissions in isotope j

$P_d(t)$ = resulting decay heat power.

If adequate substitutions are made, $\psi(t)$ can be expressed in $P_n(t)$, and a fully coupled set of equations is found.

The model described in Eqs. (6) through (9) is available in CATHARE2 with 11 decay heat groups. To

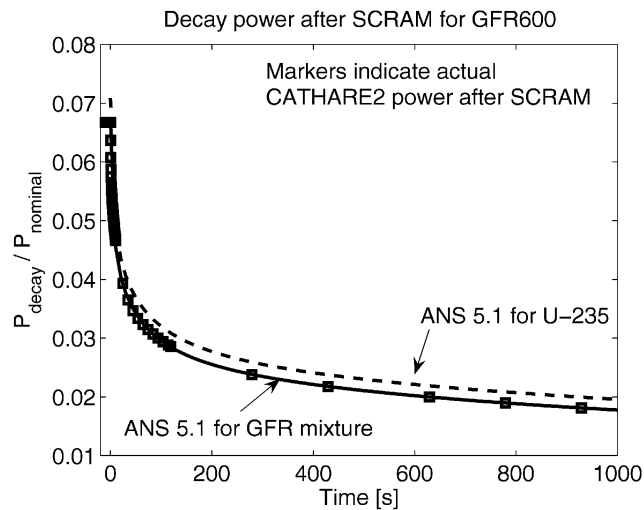


Fig. 6. Decay heat curves using ANSI/ANS-5.1-1994 (Ref. 14) for ^{235}U and a synthetic mixture for GFR600. Markers indicate CATHARE2 result for decay heat.

represent the decay heat source of the GCFR, the decay power is calculated using the ANSI/ANS-5.1-1994 law, employing a fissioning mixture with 20% fast fissions in ^{238}U , 40% fissions in ^{239}Pu , and 40% fissions in ^{241}Pu . The curve obtained in this way was fitted with an 11-group model based on Eq. (4). The resulting model gives a steady-state decay power of 6.7% of nominal power. In Fig. 6 a comparison is presented of the decay heat power from ANSI/ANS-5.1-1994 for thermal fission of ^{235}U (light water reactor), the synthetic GCFR curve, and the decay power calculated by CATHARE2 using the fitted decay heat model.

It should be noted that the decay heat curve proposed here might not be very accurate. First of all, no data are available in ANSI/ANS-5.1-1994 for fast reactors. Second, alpha decay of the MAs is not taken into account. Third, the effect of capture reactions in the actinides and subsequent decay are not treated explicitly. On the other hand, application of the model of Eqs. (6) through (9) incorporates the entire power history during a transient. The proposed model is the best possible given the currently available data on decay heat, fuel design, and material properties.

VI. RESULTS OF TRANSIENT CALCULATIONS

Three relevant corewide transients were calculated:

1. *A loss of flow at constant pressure:* An initiating event for such a transient would be the (faulty) activation of the turbocompressor braking system (the braking system prevents the turbocompressor from overspeeding, for instance due to a load rejection). As indicated in

Ref. 10, the premature stopping of the turbocompressor can be considered a worst-case scenario under pressurized conditions.

2. *Ramp insertion of reactivity:* 0.9 \$ of reactivity is introduced linearly over 20 s to simulate the faulty withdrawal of a control rod. Pressure and flow remain at steady-state values.

3. *Ramp insertion of reactivity, but now 0.9 \$ in 1 s:* to simulate the effect of a control rod ejection.

In all calculations the Doppler reactivity coefficient corresponds to a fuel with 5% MAs at beginning of cycle, i.e., $\text{FTC} = -0.56 \text{ pcm/K}$ (see third column of Table III). This is acceptable since the FTC of the irradiated fuel is of similar magnitude. Since a pressure boundary condition is used, the void reactivity coefficient is not taken into account to avoid calculating spurious reactivity effects. The LIMs are activated when the gas temperature at the outlet of (one of) the fuel assemblies surpasses 1000°C . Once the LIM is activated, introduction of the ^6Li is simulated to take 1 s. All transients were calculated assuming that one LIM is activated, which implies that the LIM worth depends on the position of the LIM. As given in Table IV, one LIM at the center position introduces $-2.10 \text{ $}$, while one LIM at an off-center position has a worth of $-1.49 \text{ $}$. An extra calculation was done in which one LIM with a smaller worth ($-1.10 \text{ $}$) is used. This calculation serves to estimate opportunities to change the LIM design.

VI.A. Loss of Flow

In this case, the coolant mass flow rate decreases as

$$\dot{m}(t) = \frac{\dot{m}_0}{1 + t_s/\tau}, \quad (10)$$

where t_s is the time since the start of the transient and $\tau = 10 \text{ s}$. The constant τ is a typical timescale for the decrease of the turbine speed. The value of $\tau = 10 \text{ s}$ has been adopted in the GCFR-STREP collaboration as a worst case, i.e., the quickest timescale for stopping the turbocompressor. With $\tau = 10 \text{ s}$, the flow is reduced to 5% of the nominal mass flow after 200 s, which is in line with the results from Ref. 10. When the mass flow in the cold duct falls below 5% of the steady-state value, the cold duct and hot duct are isolated, the valves on the DHR circuits are opened, and natural circulation is allowed to develop.

A first calculation was done for the LOFA without any control to check whether an LIM is necessary. Two calculations were done, one with the FTC as calculated for the MA fuel (-0.56 pcm/K) and one calculation with an artificial, ten-times-stronger feedback (-5.6 pcm/K). The result is given in Figs. 7 and 8. The small FTC results in a large temperature variation during the transient. A larger FTC results in a lower temperature and quicker

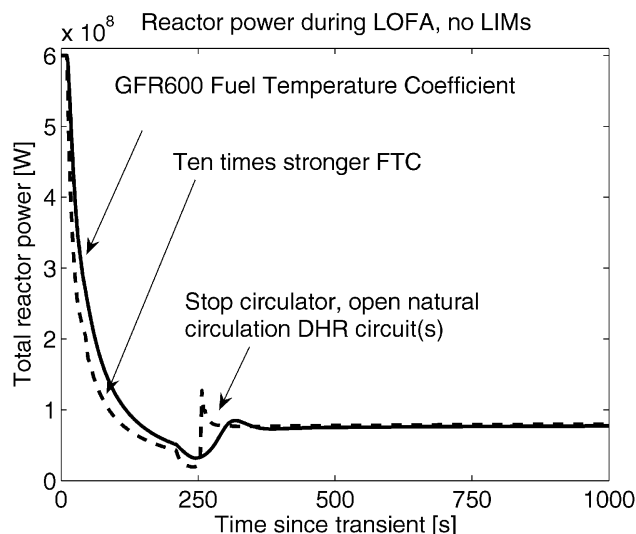


Fig. 7. Power during unprotected loss of flow. Solid line: $FTC = -0.56 \text{ pcm/K}$; dashed line: $FTC = -5.6 \text{ pcm/K}$. In the natural-circulation phase, the power is governed by the heat exchange in the DHR circuits.

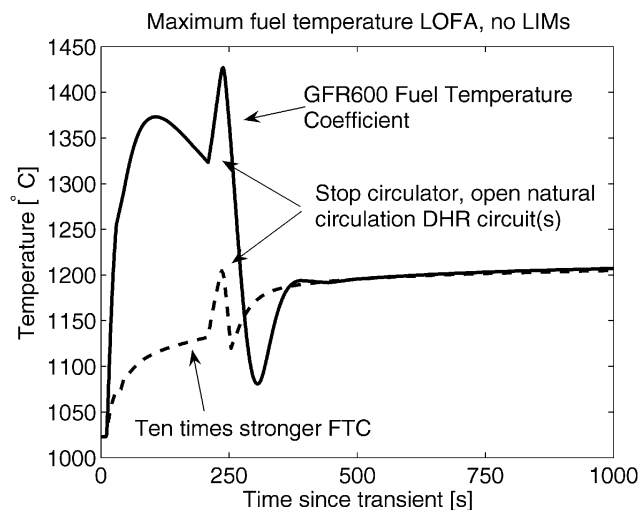


Fig. 8. Maximum fuel temperature during unprotected loss of flow. In the natural-circulation phase, the fuel temperature is dictated by the power transferred by the DHR circuits and the core inlet conditions, independent of the magnitude of the Doppler coefficient.

decrease of neutronic power, but in both cases the reactor stabilizes in the natural-circulation regime at a power of $\sim 75 \text{ MW(thermal)}$. This power is larger than the DHR loops are designed to extract [18 MW(thermal)]. In the natural-circulation phase, the fuel temperature is $\sim 1200^\circ\text{C}$, which may be within limits but is undesirable for a prolonged period. It is concluded that some reactivity control device is necessary. It may be surprising that the

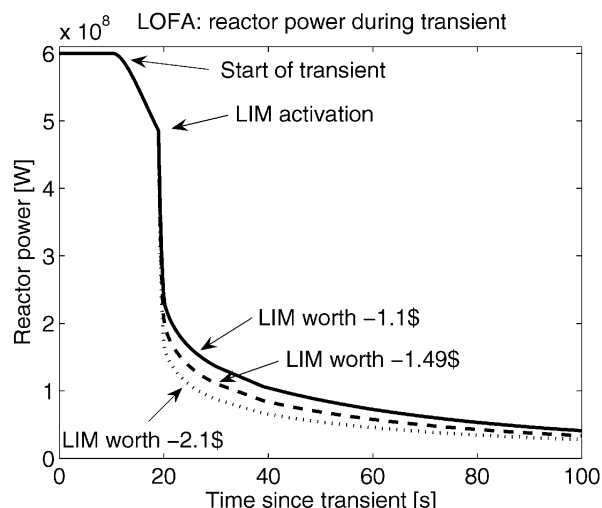


Fig. 9. Power during LIM-protected loss of flow for several LIM worths. Notice the effect of LIM worth on the prompt drop.

natural-circulation regime is insensitive to the Doppler coefficient. In natural circulation, the power transfer from the core is dictated by the natural-circulation conditions in the DHR heat exchangers. Because of the employed model, the temperature of the helium in the cold leg of the DHR loop is more or less fixed. Thus, the core inlet temperature is the same for both calculations, regardless of the Doppler coefficient. Because we have used a linear Doppler feedback model, the temperature profile established in the fuel is independent of the magnitude of the Doppler coefficient.

In Figs. 9 and 10, the result is given for LIMs of different worths. When the coolant mass flow rate into the core starts to decrease, the fuel temperature starts to increase, leading to negative reactivity due to Doppler feedback. Once the freeze seal melts, introduction of the lithium into the assemblies is rapid: The pressure difference between the storage tank and the primary system is large compared to the pressure difference over the column of ${}^6\text{Li}$. A quick calculation shows that the time required for introduction of the lithium is $\approx 0.1 \text{ s}$. In the calculation, a value of 1 s was adopted. The introduction of negative reactivity is so large that the fission chain reaction shuts down quickly. The prompt drop that occurs after activation of the LIM(s) is clearly visible in Fig. 9. Following the prompt drop, the neutronic power decrease is governed by the slowest group of delayed neutron precursors and by the decay power. For a larger worth of the LIMs, the initial drop is larger [see Eq. (3)]. This results in a lower temperature during circulator run-down. When the cross duct is isolated, and the DHR circuit is opened, a “hump” is visible in the graph (at $\sim 200 \text{ s}$). The hump is caused by a short period of flow stagnation when the cold and hot duct valves are closed.

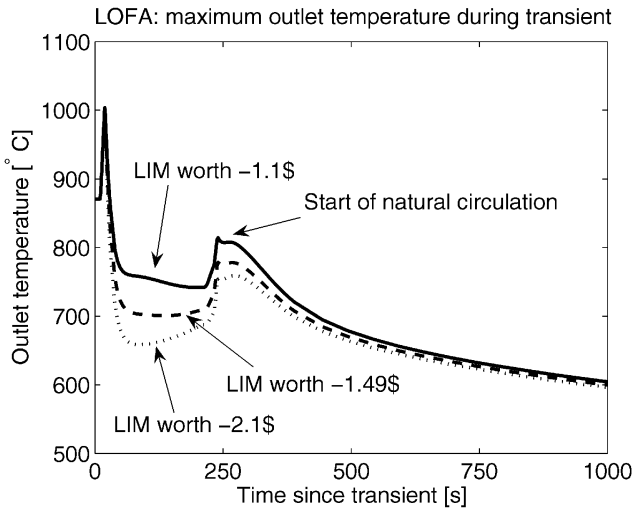


Fig. 10. Outlet temperature of the hottest fuel assembly during LIM-protected loss of flow. The hump is caused by the isolation of the turbine, followed by the opening of the DHR system.

Soon after, natural circulation is established, and temperatures in the core start to decrease. Under pressurized conditions, the DHR circuit has adequate heat removal capacity: The outlet temperature of the core decreases steadily under natural circulation. In the natural-circulation regime, heat exchanges in the system are by and large governed by the decay heat of the fuel and the natural-circulation conditions in the helium DHR loop and the secondary H₂O DHR loop and are insensitive to the LIM worth.

VI.B. Reactivity Evolution After Loss of Flow

While the core cools down, its reactivity increases because of the Doppler effect. For GFR600, the reference fuel temperature used to calculate the magnitude of the Doppler effect is 858°C (steady-state value). There are three plausible values of the final temperature of the core after SCRAM:

1. 480°C, the steady-state inlet coolant temperature: This introduces +212 pcm (0.57 \$) of reactivity.
2. 90°C, the temperature of the water in the secondary branch of the DHR circuits: This introduces +430.1 pcm (1.15 \$) of reactivity.
3. 25°C, the ambient temperature: This introduces +466.5 (1.25 \$) of reactivity.

These values are calculated based on β of the GFR600 fuel with 5% MAs. The Doppler effect is stronger for the standard mixed oxide fuel, leading to larger reactivity effects during cooldown. In Figs. 11 and 12, the Doppler

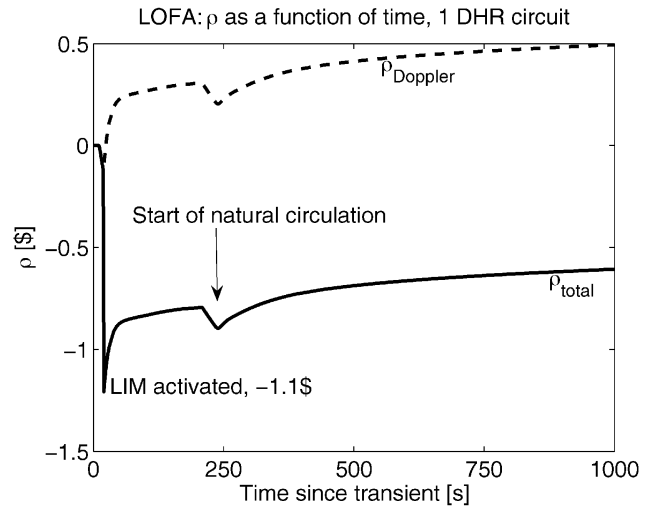


Fig. 11. Doppler and total reactivity during LIM-protected loss of flow; LIM worth = -1.10 \$. The total reactivity is negative during the transient. One DHR loop is active.

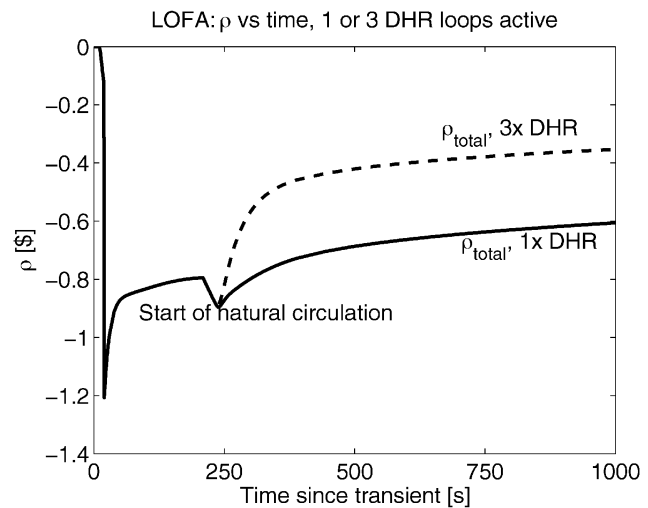


Fig. 12. Comparison of total reactivity during LIM-protected loss of flow, LIM worth = -1.10 \$, with either one or three DHR loops active. With three active DHR loops, the core cools down quickly, leading to a smaller reactivity margin.

reactivity and total reactivity are given for an LIM worth of -1.10 \$.

The primary system is equipped with three redundant DHR loops, each capable of extracting 3% of nominal power under pressurized conditions. If all three loops are activated, the primary system will cool down much faster than when only one loop is activated. As a result, reactivity effects due to Doppler feedback will have a different timescale. Figure 12 illustrates this effect. If

one DHR loop is activated, the rate at which the core cools down is such that after 1000 s the reactivity is about -0.6 \$, but with all three DHR loops active, the reactivity is smaller than -0.4 \$ at 1000 s. In the calculations presented here, the temperature of the ultimate heat sink is 90°C , so with an LIM worth of -1.10 \$, the core will become critical again. The moment of recriticality is determined by the number of active DHR loops, but even a low-worth LIM would yield several thousands of seconds' grace time to take action before recriticality occurs. It should be noted that the three parallel DHR loops have a potential for unstable flow distribution (no instabilities occurred in the calculations). The current design philosophy is to have three loops for redundancy, in spite of potential instabilities.

VI.C. Ramp Reactivity Introduction

For this scenario, the results are summarized in Figs. 13 and 14. In all cases, one LIM would be sufficient to limit the reactor power. If one LIM is activated, a certain amount of negative reactivity is introduced, and together with the $+0.9$ \$ due to control rod movement and the Doppler feedback, a net reactivity is established. During this transient it is assumed that the coolant inlet conditions remain at steady-state values. Hence, the lowest temperature the fuel can attain is 480°C . As shown in Sec. VI.B, cooling down the fuel to 480°C increases reactivity by 0.57 \$. It is concluded that an LIM worth >0.9 \$ $+0.57$ \$ will shut down the reactor. A lower LIM worth will establish a new power level in the reactor,

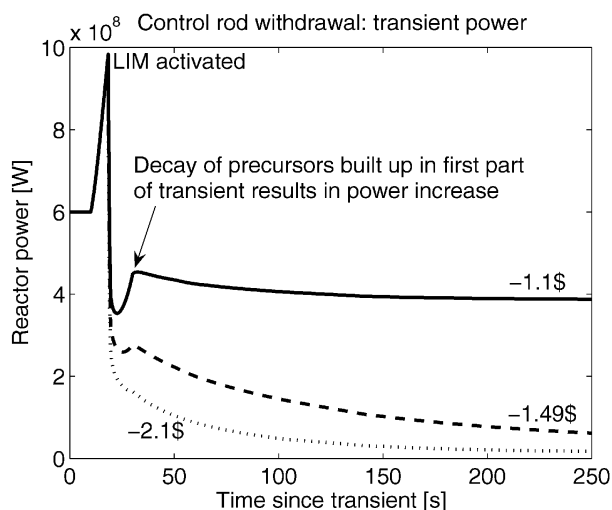


Fig. 13. Power during LIM-protected CRW ($+0.9$ \$ in 20 s). If the LIM is strong enough (>1.47 \$, roughly), shutdown is achieved. For a lower worth, a new power level is established, where the effects of Doppler feedback, control rod reactivity, and LIM reactivity counterbalance each other to give $\rho = 0$.

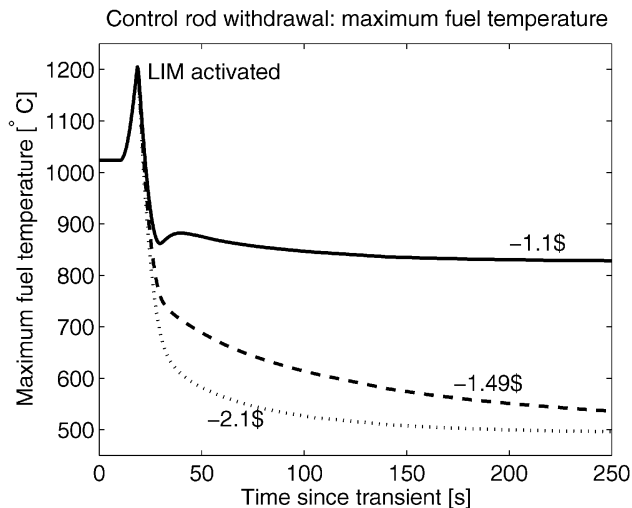


Fig. 14. Maximum fuel temperature during LIM-protected CRW.

where the Doppler feedback, LIM worth, and control rod worth determine the final state.

VI.D. Control Rod Ejection

A calculation was done simulating a control rod ejection, where the control rod moves out of the core in 1 s. In Figs. 15 and 16, the results are given for the reactor power and the maximum fuel temperature. Note that the power peaks at almost six times the nominal power. The maximum temperature of the fuel is not much higher than in the previous case, $\sim 1350^{\circ}\text{C}$.

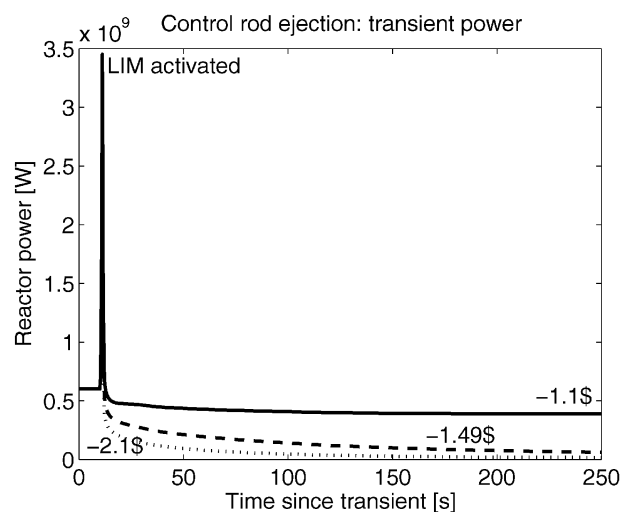


Fig. 15. Power during LIM-protected control rod ejection ($+0.9$ \$ in 1 s). Note the power peak, which reaches almost six times nominal power.

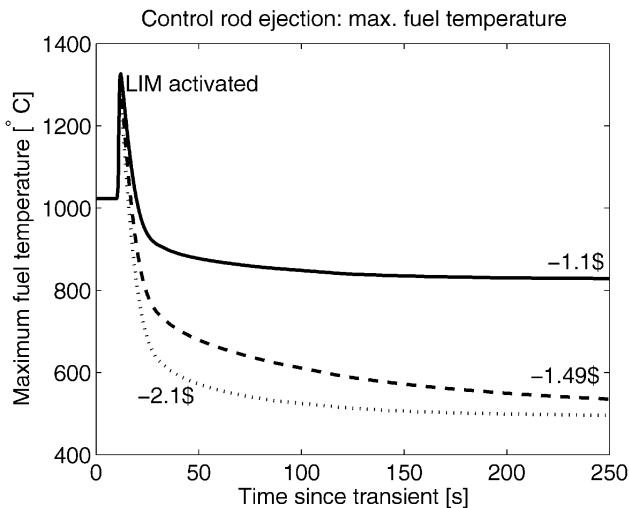


Fig. 16. Maximum fuel temperature during LIM-protected control rod ejection. Note that although the power peaks at almost six times nominal, the maximum fuel temperature is only 100 K higher than in the CRW case.

From Figs. 15 and 16, the long-term behavior of the reactor after the control rod ejection is not much different from the CRW case, but the beginning of the transient is much steeper, with a very rapid increase of power production and temperatures. This causes concern for material degradation by thermal shock. It should be noted that if an active SCRAM system is used, the resulting transient would be similar to the result given here.

VII. CONCLUSION

In this paper a passive device is proposed to limit the reactor power output of a GCFR under off-nominal conditions when other control elements have failed. From the investigations presented in this paper, the following conclusions are drawn:

1. LIMs are capable of controlling the power production in the reactor, even if a large reactivity is accidentally inserted (+0.9 \$). If only one LIM is activated, the reactor may not be shut down completely, but the power production remains bounded.
2. The precise requirement for the worth of one LIM cannot yet be determined. The required worth depends on several design parameters, which are not yet known: the worth of one control rod, the pressure holding system, and the lowest fuel temperature reached in a transient. However, from the calculations presented in Sec. VI.B, it is clear that even a rather low worth (−1.10 \$) will protect the fuel from excessive temperatures.

3. If a temperature-controlled passive control element is present in the core, it is highly likely that only one LIM will be activated because the prompt jump in power caused by LIM operation will decrease temperatures below the activation temperature of the other LIMs. Redundancy may call for more than one LIM in the core.

4. A temperature-controlled passive device will only detect off-nominal conditions occurring in a neighboring fuel assembly.

5. Transients initiated by faulty control rod movement and followed by a quick response of the active or passive control system result in rapid transients of power and temperatures. Degradation of ceramic structural materials might become problematic in these cases.

VIII. DISCUSSION

Once a more detailed design of the LIM is available, a laboratory-scale prototype should be made to assess the important factors such as freeze seal venting, sealing capability of the SiC pistons, Rayleigh-Taylor stability under transient conditions, etc. Also, a list of probable initiating events for LIM failure should be prepared if and when a more detailed design is available. The presence of the LIMs in the core may introduce new (extra) modes of failure. An example could be the spurious activation of an LIM or the breach of one of the LIM tubes. The risks of the presence of the LIMs are currently difficult to evaluate, as this requires a detailed design of the LIMs. Other passive systems that could be considered are a rotating drum with B₄C particles, which is driven by the flow. If the flow stops, the drum stops rotating, and the particles drop into the core.

The employed numerical models still lack some more or less important effects, the most obvious being the lack of a model for the power conversion unit. Other uncertainties are a lack of material data for the SiC fuel plates, reflector and shielding design within the fuel assemblies, and a realistic model for the H₂O DHR loops. Future research should therefore focus on an adequate model of the power conversion unit. A detailed calculation should be performed to estimate ⁶Li depletion and tritium formation during irradiation. A detailed mechanical design of the freeze seals should be made to estimate how much material is required. For example, a considerable pressure difference acts on the freeze seals, especially during partially pressurized conditions, for instance during refueling. With the amount of material known, it is possible to estimate how long it would take to melt the seals. The response to loss of flow should be analyzed for several timescales. For instance, a turbine deblading accident could cause a very rapid loss of flow. However, it is the authors' opinion that for such an accident, as well as for

an LB-LOCA, passive reactivity control by itself is not sufficient to prevent core damage.

ACKNOWLEDGMENTS

The authors would like to acknowledge the support of the European Commission. The GCFR STREP is carried out under contract 012773 (FI60) within the EURATOM 6th Framework Programme (<http://www.cordis.lu/fp6/>), effective from March 1, 2005, to February 28, 2009. More information about the GCFR STREP is available from the project Web site (<http://www.gcfr.org>). We would like to thank P. Dumaz and C. Poette of CEA for providing details of the GFR600 primary system, and G. Lavalie and G. Geffraye for their help in obtaining CATHARE2.

REFERENCES

1. "A Technology Roadmap for Generation IV Nuclear Energy Systems," U.S. DOE Nuclear Energy Research Advisory Committee and the Generation IV International Forum, available online at <http://gif.inel.gov/roadmap/> (2002).
2. A. M. OUGOUAG, R. R. SCHULTZ, W. K. TERRY, and A. G. STEPHENS, "Preliminary Investigation of an Optimally Scramming Control Rod for Gas-Cooled Reactors," *Proc. 10th Int. Conf. Nuclear Engineering (ICONE-10)*, Arlington, Virginia, April 14–18, 2002, American Society of Mechanical Engineers (2002).
3. A. M. OUGOUAG, W. K. TERRY, and R. R. SCHULTZ, "Conceptual Design of a Passive, Inherently Safe Emergency Shutdown Rod for High-Temperature Reactor Applications," *Proc. Conf. High Temperature Reactors (HTR2002)*, Petten, The Netherlands, April 22–24, 2002, European Nuclear Society/International Atomic Energy Agency (2002).
4. K. O. OTT and R. J. NEUHOLD, *Introductory Nuclear Reactor Dynamics*, American Nuclear Society, La Grange Park, Illinois (1985).
5. "SCALE: A Modular Code System for Performing Standardized Computer Analyses for Licensing Evaluations, ORNL/TM-2005/39, Version 5, Vols I-III," Oak Ridge National Laboratory (2005); available from Radiation Safety Information Computational Center at Oak Ridge National Laboratory as CCC-725.
6. J. L. KLOOSTERMAN and J. C. KUIJPER, "VAREX, A Code for Variational Analysis of Reactivity Effects: Description and Examples," *Proc. Int. Mtg. Mathematical Methods for Nuclear Applications (M&C 2001)*, Salt Lake City, Utah, September 2001, American Nuclear Society (2001) (CD-ROM).
7. M. KAMBE and M. UOTANI, "Design and Development of Fast Breeder Reactor Passive Reactivity Control Systems: LEM and LIM," *Nucl. Technol.*, **122**, 179 (1997).
8. "Safety Related Terms for Advanced Nuclear Plants," IAEA-TECDOC-626, International Atomic Energy Agency (1991).
9. E. GUYON, J.-P. HULIN, L. PETIT, and C. D. MITESCU, *Physical Hydrodynamics*, Oxford University Press, New York (2001).
10. N. TAUVERON, M. SAEZ, M. MARCHAND, T. CHATAING, G. GEFFRAYE, and C. BASSI, "Transient Thermal-Hydraulic Simulations of Direct Cycle Gas Cooled Reactors," *Nucl. Eng. Des.*, **235**, 2527 (2005).
11. F. MORIN, T. CADIOUT, C. POETTE, A. TOSELLO, and Y. ENUMA, "Preliminary Design of ETDR, D10 Task 1.2," GCFR-STREP Deliverable D10, Commissariat à l'Énergie Atomique (2006).
12. H. BAILLY, D. MÉNESSIER, and C. PRUNIER, "The Nuclear Fuel of Pressurized Water Reactors and Fast Reactors," Lavoisier Publishing, Inc., Secaucus, New Jersey (1999).
13. G. LAVIALLE, "CATHARE 2 v2.5 mod3.1 User's Manual," CEA S8TH/LDAS/EM/2005-035, Commissariat à l'Énergie Atomique (2006).
14. "Decay Heat Power in Light Water Reactors," ANSI/ANS-5.1-1994W2004, American Nuclear Society (2004).
15. "Berechnung der Nachzerfallsleistung der Kernbrennstoffe von Leichtwasserreaktoren; Nichttrezyklierte Kernbrennstoffe," DIN 25463-1, Deutsches Institut für Normung e.V. (1990).
16. K. TASAKA, J. KATAKURA, H. IHARA, T. YOSHIDA, S. IJIMA, R. NAKASIMA, T. NAKAGAWA, and H. TAKANO, "JNDC Nuclear Data Library of Fission Products, Second Version," JAERI-1320, Japan Atomic Energy Research Institute (1990).